Spatiotemporal Relationships Among Early Events of Fertilization in Sea Urchin Eggs Revealed by Multiview Microscopy

Keisuke Suzuki,* Yuriko Tanaka,* Yoko Nakajima,‡ Ken'ichi Hirano,§ Hiroyasu Itoh,§ Hidetake Miyata,* Tsuyoshi Hayakawa,§ and Kazuhiko Kinosita, Jr.*

*Department of Physics, Faculty of Science and Technology, and ‡Department of Biology, Keio University, Hiyoshi, Kohoku-ku, Yokohama 223; and §Tsukuba Research Laboratory, Hamamatsu Photonics K. K., Tokodai, Tsukuba 300–26, Japan

ABSTRACT Four early events of egg fertilization, changes in intracellular calcium concentration and intracellular pH, reorientation of the surface membrane, and the elevation of the fertilization envelope, were imaged in real time and in pairs in single sea urchin eggs. The paired imaging allowed the correlation of the four events spatially and temporally. Three of them propagated as waves starting at the sperm entry site. The earliest was the calcium wave, visualized with fluorescent indicator dyes. After a delay of 10 s there followed a large decrease in the fluorescence polarization of membrane-bound dyes, which we interpret as arising from membrane reorientation as a result of cortical granule exocytosis and microvillar elongation. With a further delay of 15 s the fertilization envelope was seen to rise in transmitted light. All three waves propagated with similar velocities of ~10 μm/s, supporting the view that calcium triggers the latter two events. The fluorescence polarization changed in two steps with a clear pause of 10–20 s in between. The second step, which also propagated as a wave, reflects either further elongation of microvilli or straightening of irregular microvilli. This second step was abolished by cytochalasin B and was coincident with an increase in cytoplasmic pH, suggesting that pH-induced actin reorganization may play a role. The cytoplasmic alkalinization, imaged with a fluorescent probe, was quite different from the other events in that it took place homogeneously throughout the egg and slowly (over 100 s). Apparently, the alkalinization is not on a direct downstream pathway of calcium origin. An opposing possibility, that the alkalinization may in fact be triggered by the traveling calcium wave, is also discussed.

INTRODUCTION

Fertilization by sperm induces multiple series of events that eventually lead to the activation of the developmental machinery of the egg. In the sea urchin egg, the earliest detectable event after sperm binding is membrane depolarization (Steinhardt et al., 1971; Chambers and de Armendi, 1979) simultaneous with the fusion of the sperm and egg membranes (McCulloh and Chambers, 1992). The calcium wave, transient rise in the intracellular free calcium concentration $[Ca^{2+}]_i$, then propagates across the egg cytoplasm (for reviews see Jaffe, 1985; Whitaker and Swann, 1993; Berridge, 1993). At the egg surface, the calcium wave triggers the fusion of cortical granules with the plasma membrane, followed by the elongation of microvilli and the formation and elevation of the fertilization envelope (for reviews see Schuel, 1985; Kay and Shapiro, 1985; Chandler, 1991). In the cytoplasm, pH gradually increases, which is an essential component of egg activation (Johnson et al., 1976; Shen and Steinhardt, 1978).

All of these early events have been studied extensively and are well established at the phenomenological level. However, the underlying molecular mechanism and the signaling pathways linking individual events are not yet fully clear. To disentangle the molecular interplay in a fertilizing egg, it is highly desirable to make real-time and simultaneous observations of different events in individual, living eggs under normal and perturbed conditions. Combining video microscopy with microelectrode techniques, Eisen et al. (1984) were able to correlate five early events of fertilization: membrane depolarization, surface contraction, calcium wave, elevation of fertilization envelope, and increase in pyridine nucleotide fluorescence. Hamaguchi and Hamaguchi (1990) modified a microscope and succeeded in simultaneous imaging of calcium dynamics and morphological changes. Attempts at combined measurements, however, have been relatively scarce.

In this paper, we describe spatial and temporal relationships among four early events of fertilization: changes in $[Ca^{2+}]_i$ and intracellular pH, reorientation of surface membrane resulting from cortical granule exocytosis and microvillar elongation, and elevation of the fertilization envelope. We imaged these events in pairs, using multiview microscopy, which is an extension of the dual-view version reported previously (Kinosita et al., 1991). $[Ca^{2+}]_i$ and intracellular pH were imaged with fluorescent indicators, and the fertilization envelope was directly observed in a transmission image. The membrane reorientation was assessed from the changes in the fluorescence polarization of membrane-bound probes: the reorientation of the surface membrane resulted in the reorientation of the direction of polarization.

Received for publication 18 July 1994 and in final form 21 December 1994.

Address reprint requests to Dr. Kazuhiko Kinosita, Jr., Department of Physics, Faculty of Science and Technology, Hiyoshi 3–14–1, Kohoku-ku, Yokohama 223, Japan. Tel.: 81-45-563-1141; Fax: 81-45-563-1761;

0006-3495/95/03/739/10 $2.00

MATERIALS AND METHODS

Gametes

Gametes of the sea urchin *Anthocidaris crassispina* were obtained by applying an alternating current at ~30 V to the animal body through carbon

electrodes. Gametes from the sand dollar *Scaphechinus mirabilis* were obtained by intracelomic injection of 0.1 M acetylcholine chloride. The two species gave qualitatively similar results. Data reported in this paper refer to *A. crassispina* unless explicitly stated otherwise.

Eggs were dejellied by washing them four times in a Ca^{2+}-free sea water (Jamarine Laboratories, Osaka, Japan). Handling and observation of the eggs were made at 21 ± 2°C, in artificial sea water (ASW, Jamarine Laboratories) titrated to pH 8.0 except where stated otherwise. Sperm were kept "dry" at 0°C and diluted 500–1000× with ASW before use.

In some experiments, the vitelline coat of unfertilized eggs was removed by treating the dejellied eggs with 10 mM dithiothreitol (DTT, pH 9.2 in ASW) for 3 min (Epel et al., 1970). In one experiment, eggs of *S. mirabilis* treated with DTT were further treated with cytochalasin B (Sigma Chemical Co., St. Louis, MO); the eggs were incubated in 20 μM cytochalasin B in ASW (addition from 20 mM stock in DMSO) for 10 min, washed once with ASW, and used immediately.

Fluorescence staining and observation chamber

To observe $[Ca^{2+}]_i$ and intracellular pH, the eggs were microinjected with one of the following dye solutions: 0.2–0.4% of the egg volume of 5 mM Calcium Green-1 (Molecular Probes, Inc., Eugene, OR) in 500 mM Hepes at pH 7.2, 0.4–0.9% egg volume of 3 mM indo-1 (Dojindo Laboratories, Kumamoto, Japan) in water, or 0.8–1.3% egg volume of 1.6 mM carboxy SNARF-1 (Molecular Probes, Inc.) in water. The plasma membrane of the eggs was stained by soaking the eggs in 3 μM *N*-(3-(triethylammonium)-propyl)-4-(4-(*p*-dibutyl-aminophenyl)butadienyl)-pyridinium dibromide (RH292, Molecular Probes, Inc., Eugene, OR) in ASW. In some experiments, the membrane was stained with 1,1′-dihexadecyl-3,3,3′,3′-tetramethylindocarbocyanine perchlorate (diI, Molecular Probes, Inc.) by the following procedure: ethanolic solution of the dye (3 mg/ml) was diluted 120-fold into warm (30–40°C) water containing 1.2 M sucrose, 1 mM KCl, and 0.1 mM Tris at pH 8. After sonication for 30 s and cooling, eggs in ASW were gently added on top of the dye suspension and incubated for 1 min. The eggs lying just above the interface were then collected with a pipette and washed with ASW.

An observation chamber was made with a large (bottom) and a small (top, 8 × 12 mm^2) coverglass. The spacers between the two were made in such a way that the top coverglass was slightly slanted and the vertical spacing at the center was approximately the egg diameter (100 μm). An egg, either microinjected or stained with RH292 or diI, was introduced into the chamber from the larger opening by sucking the medium (ASW), with a piece of filter paper, from the other side until the egg rested still in the middle, slightly pressed between the coverglasses. In the case of eggs stained with RH292, the dye remaining in the medium was removed by further infusion of dye-free ASW.

In experiments where $[Ca^{2+}]_i$ and the membrane were simultaneously imaged, an egg microinjected with Calcium Green-1 was stained with RH292 in the observation chamber: ASW containing 3 μM RH292 was slowly infused until the fluorescence intensity of RH292 reached a level that would match that of Calcium Green-1 during the propagation of the calcium wave. Excess RH292 in the medium was then removed by infusion of dye-free ASW.

For fertilization, a dilute sperm suspension was infused from the larger opening and sucked from the other side with a piece of filter paper. Sperm reached the egg within a few seconds.

Multiview microscopy

A version of dual-view microscopy, termed "W-microscopy," has been described (Kinosita et al., 1991), in which two different images of an object can be observed simultaneously and continuously through a single video camera. A beam separator inserted between the microscope body and the camera separates the image-forming beam into two component beams according to the wavelength or the direction of polarization. The two beams are deviated from each other by a few degrees, making two images side by side on the camera.

In the present work, we observed three different images simultaneously by inserting two sets of chevron-type beam separators (Kinosita et al., 1991) in tandem (Fig. 1). One set deviated the separated beams into up and down directions and the other into right and left, making four images arranged in a two-by-two format. One of the four images was redundant in the present observations (e.g., transmission image or the fluorescence of Calcium Green-1 were insensitive to the direction of polarization) and was therefore not used in the analyses.

Various optical setups used are summarized in Table 1. Inverted microscopes, either Carl Zeiss ICM-405 (Tokyo, Japan) or Nikon Diaphot TMD (Tokyo, Japan), were used with an objective Nikon Fluor 20 (NA 0.75). Excitation source for fluorescence was a 100-W, high-pressure mercury lamp. To reduce photobleaching, the excitation intensity was reduced with Zeiss neutral density filters. For polarization imaging with Nikon TMD, excitation light was completely unpolarized by canceling the slight polarization, introduced by the dichroic mirror that reflected the excitation light, with two pieces of coverglass placed obliquely in the excitation beam. With Zeiss ICM-405, the polarization of the excitation light was found to be negligible. To achieve wavelength separation as listed in Table 1, we used dichroic mirrors and filters obtained from Carl Zeiss, Nikon, Asahi Spectra Co., Ltd. (Tokyo, Japan), Kawai Optics, Co., Ltd. (Shizuoka, Japan), Fuji Film Co., Ltd. (Tokyo, Japan), and Hoya Co., Ltd. (Tokyo, Japan). Separation of emitted fluorescence into vertically and horizontally polarized components was achieved with a broad-band polarizing beam splitter from Sigma Koki Co., Ltd. (Saitama, Japan).

Images were captured with a silicon-intensified target camera (either C1000 or C2741, Hamamatsu Photonics K. K., Shizuoka, Japan) and recorded on an S-VHS video recorder (either A-VS-1, Toshiba Co., Ltd., Tokyo, Japan, or NV-FS1000, Matsushita Electronics, Co., Ltd., Tokyo, Japan). The recorded images were analyzed with a digital image processor (Hamamatsu C2000). Corrections for image distortion and shading were done as described (Kinosita et al., 1991). An image of a rectangular grid was used for the distortion correction. For shading corrections, dye solutions were imaged as homogeneous references; in the case of RH292, a suspension of asolectin liposomes stained with RH292 was used as the reference. All fluorescence images were corrected for the background: an image of blank medium adjacent to the egg was subtracted. Autofluorescence of the eggs was ignored. The intensity of the autofluorescence relative to the dye signal was at most 1% for RH292, 4% for Calcium Green-1, 3% for carboxy SNARF-1, and 10% for indo-1.

Electron microscopy

For the observation of microvilli, the vitelline coat of unfertilized eggs was removed by the DTT treatment. At various times after fertilization, the eggs were fixed in the mixture of 1 volume of 8% glutaraldehyde and 7 volumes of ASW, and postfixed with 0.5% OsO_4 in 0.35 M sodium acetate. After dehydration with ethanol, the specimens were critical-point dried in CO_2,

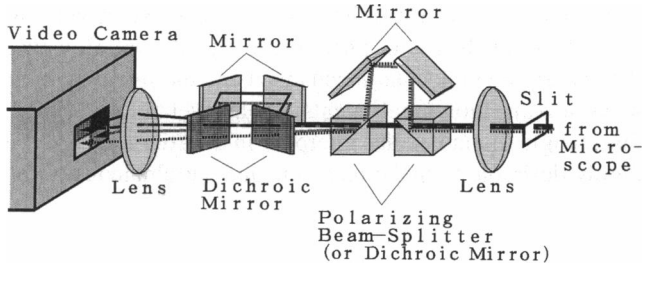

FIGURE 1 Optical system for multiview microscopy. A rectangular mask, shown at the right, was placed on the intermediate image formed at the camera port of a microscope (Zeiss ICM-405 or Nikon TMD). The central quadrant of the intermediate image passed through the slit, separated and deviated by the two sets of beam separators, and refocused on the camera in a two-by-two format.

TABLE 1 Optical setups used in the multiview microscopy

Image sets	Fluorescence excitation	Transmission light source	First beam separator	Second beam separator
(1) Fertilization envelope and membrane orientation				
Transmission		400–450 nm	v-polarized*	400–450 nm
RH292‡ (v-polarized)	520–540 nm		v-polarized	>600 nm
RH292‡ (h-polarized)	520–540 nm		h-polarized	>600 nm
(2) $[Ca^{2+}]_i$ and membrane orientation				
Calcium Green-1	435–495 nm		v-polarized*	500–560 nm
RH292 (v-polarized)	435–495 nm		v-polarized	>620 nm
RH292 (h-polarized)	435–495 nm		h-polarized	>620 nm
(3) Fertilization envelope and pH				
Transmission		430–450 nm	<600 nm	400–450 nm
SNARF-1 (>600 nm)	500–512 nm		>600 nm	600–660 nm
SNARF-1 (<600 nm)	500–512 nm		<600 nm	525–600 nm
(4) $[Ca^{2+}]_i$ and fertilization envelope				
Transmission		>685 nm	>685 nm	
Calcium Green-1	435–495 nm		510–570 nm	
(5) $[Ca^{2+}]_i$				
Indo-1 (>455 nm)	335–350 nm		>455 nm	
Indo-1 (<455 nm)	335–350 nm		<455 nm	

Abbreviations: h, horizontal; v, vertical.

*h-polarized component was indistinguishable from the v-component.

‡When the membrane was stained with dil, emission between 580 and 620 nm was observed.

spatter coated with gold, and examined in a Hitachi S510 scanning electron microscope (Tokyo, Japan) at 25 kV.

RESULTS

Detection of membrane reorientation by polarized fluorescence imaging

The dye RH292 is an amphipathic molecule with a hydrophilic head and two hydrophobic tails. The chromophoric part is expected to be inserted perpendicularly into the cell membrane, as shown diagrammatically in Fig. 2 *A*. In an unfertilized egg whose surface is relatively smooth, therefore, the fluorescence of RH292 will be polarized parallel to the egg radius (Fig. 2 *B*). When microvilli grow after fertilization, parts of the cell membrane are rotated by 90° to form the side walls of the microvilli (Fig. 2 *C*). The fluorescence will then be depolarized. If the microvilli grow long and dense enough, even a reversal of polarization is expected: the direction of polarization will become perpendicular to the egg radius.

The above expectation was confirmed experimentally as seen in Fig. 3. The direction of polarization of RH292 in the cell membrane of an unfertilized egg was parallel to the egg radius (Fig. 3, *A* and *B*). Two min after insemination, the polarization became perpendicular to the egg radius (Fig. 3, *E* and *F*), indicating that a larger part of the cell membrane had been reoriented parallel to the egg radius. By this time, the egg was surrounded by a fertilization envelope as seen in Fig. 3 *G*. (The height of the fertilization envelope was relatively low, ~5 μm, in this species.)

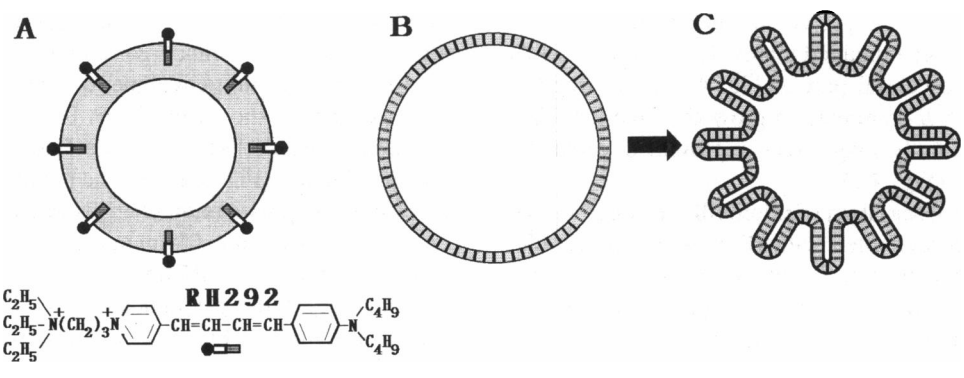

FIGURE 2 Detection of microvillar growth via fluorescence polarization of RH292. (*A*) The structure of RH292 and its presumed orientation in the cell membrane. The chromophoric part in the middle will on average be perpendicular to the membrane surface. (*B*) In a spherical cell membrane, RH292, shown by short bars, will be oriented radially. The fluorescence will therefore be polarized in the radial directions: the vertically polarized component of the fluorescence will be bright at the top and bottom of the sphere, and the horizontal component will be bright at the right and left. (*C*) When parts of the cell membrane protrude in the form of microvilli, the fluorescence will be depolarized. If the contributions from the side walls of the microvilli dominate the fluorescence signal, the direction of the polarization will become perpendicular to the radius.

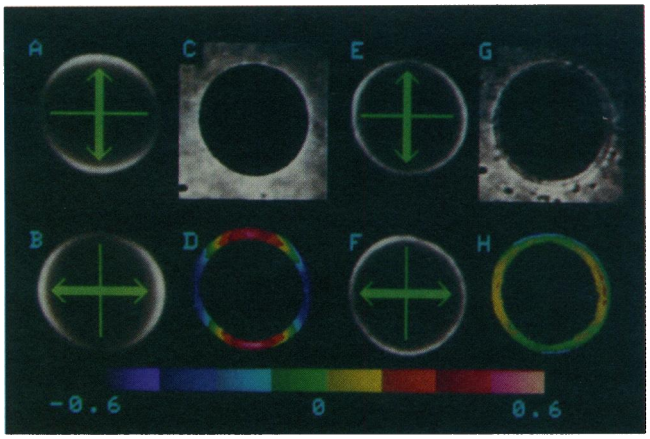

FIGURE 3 Triple-view images of an egg stained with RH292. (*A–D*) Before insemination. (*E–H*) 2 min after insemination. (*A, B, E, F*) Fluorescence of RH292. Excitation was with unpolarized light, and the emission was resolved into two orthogonally polarized components as shown by thick arrows. (*C, G*) Transmission images. The fertilization envelope did not rise uniformly in this egg (*G*). (*D, H*) Polarization of RH292 fluorescence calculated as $D = (A - B)/(A + B)$ and $H = (E - F)/(E + F)$. The polarization values are shown in false color defined in the color bar. Images except (*D*) and (*H*) are raw images.

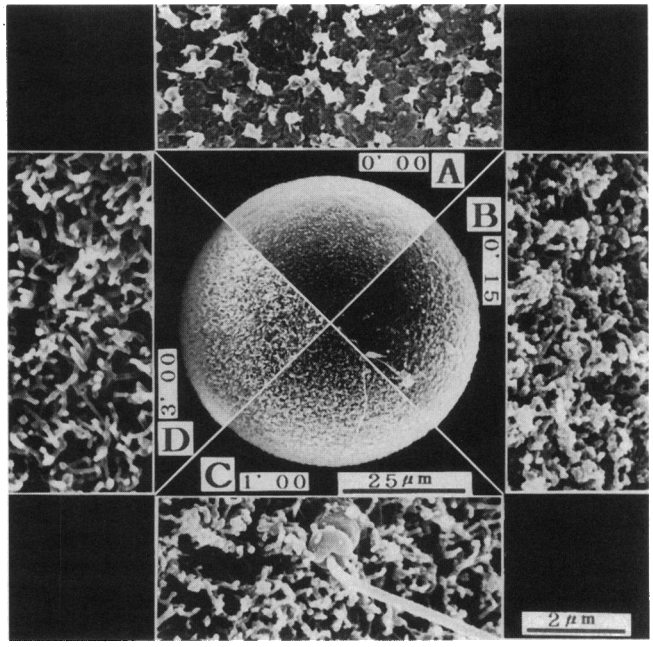

FIGURE 4 Scanning electron micrographs showing the changes in surface morphology upon fertilization. The eggs (*A. crassispina*) pretreated with DTT were fixed at the indicated times (*min's*) after insemination. Each of the four rectangular images is a magnified view of the neighboring quadrant. A fertilizing sperm is seen in (*C*) (the magnified image here is rotated relative to the central image).

The color-coded images (Fig. 3, *D* and *H*) show the degree of polarization defined as $(v - h)/(v + h)$, where v is the fluorescence intensity of the vertically polarized component (Fig. 3, *A* or *E*), and h the intensity of the horizontal component (Fig. 3, *B* or *F*). The colors also represent the orientation of RH292: warm colors imply vertical orientations, and cold colors horizontal. Reorientation of the dye molecules and hence of the cell membrane upon fertilization is easier to see in these color-coded images.

The electron micrographs in Fig. 4 show that the growth of microvilli in fact took place during the 2-min interval. The surface of an unfertilized egg shown in the top quadrant (Fig. 4 *A*) appears relatively smooth, although the magnified view shown above reveals surface irregularities (see below). By 15 s after insemination, microvilli started to grow as seen in Fig. 4 *B*. The growth did not take place uniformly on the surface. On this particular egg, the growth started at the 3:00–4:00 position; the other area remained relatively smooth at 15 s as may be seen in the central part of Fig. 4 *B*. The irregular microvilli in Fig. 4 *B* continued to grow over the next few minutes, and eventually long, erect microvilli covered the whole egg surface (Fig. 4 *D*).

To facilitate the observation of microvilli, the eggs shown in Fig. 4 had been pretreated with DTT, which blocks the formation of the fertilization envelope (Epel et al., 1970). The irregular surface of the unfertilized egg seen in Fig. 4 *A* was the result of this treatment. Without DTT, the surface appeared to be decorated with short papillae (not shown), quite similar to those described by Schroeder (1979) for an unfertilized egg of *Strongylocentrotus purpuratus*. Despite the different appearance in the electron micrographs, the DTT treatment did not significantly affect the fluorescence polarization of RH292: the absolute values of polarization at the top, bottom, right, and left of unfertilized eggs were 0.48 ± 0.05 without DTT (five eggs) and 0.41 ± 0.10 with DTT (four eggs).

Multiview images

In Fig. 3, we observed the membrane reorientation (growth of microvilli) and the elevation of the fertilization envelope simultaneously, using optical setup 1 in Table 1. Other setups allowed paired observations of $[Ca^{2+}]_i$ and membrane reorientation (2), intracellular pH and the fertilization envelope (3), and $[Ca^{2+}]_i$ and the fertilization envelope (4). These paired observations allowed us to align the four events, the calcium wave, membrane reorientation, pH change, and the rise of fertilization envelope, on the same time axis.

An example is shown in Fig. 5. Here, the top two rows, the calcium wave observed in the fluorescence images of Calcium Green-1 (Fig. 5 *A*) and the membrane reorientation detected as the polarization changes in RH292 fluorescence (Fig. 5 *B*), were obtained from one egg. A different egg gave the bottom two rows, pH images (Fig. 5 *C*, obtained with ratio-imaging of the pH indicator dye SNARF-1) and the transmission images (Fig. 5 *D*). In this figure, the AB and CD pairs are aligned with each other on the basis of the temporal relationships (see Fig. 7, below) established by the altogether four kinds of paired observations.

Three of the four events shown in Fig. 5 propagated as waves. The calcium wave (Fig. 5 *A*) was the earliest, followed by the depolarization of RH292 fluorescence

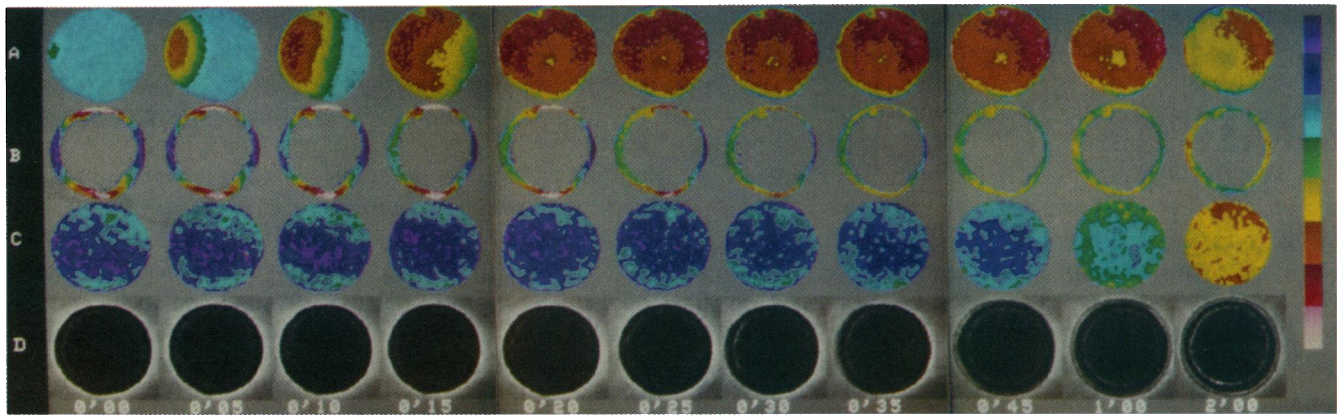

FIGURE 5 Multiview images showing spatiotemporal patterns of four early events of fertilization. Time (*min's*) zero is the time at which the calcium wave in (*A*) started on the left side of the egg. Each image here is an average over 32 frames (1.1 s). (*A*) $[Ca^{2+}]_i$ detected with Calcium Green-1. Fluorescence images were obtained with optical setup 2 in Table 1. Each image was then divided, pixel by pixel, by an image acquired before fertilization. The relative intensities thus obtained are linearly color-coded as defined in the color bar, the scale being 0 (violet) to 3 (white). The relative intensity tends to be lower at the very edge of the images, because of slight spillover of the RH292 fluorescence, which was not negligible in the relatively dark denominator image. Photobleaching of Calcium Green-1 was 0.7%/min and is therefore negligible. (*B*) Membrane reorientation as detected in the polarization of RH292 fluorescence. These images were taken simultaneously with (*A*). The color-coded polarization values (violet for −0.35 and white for 0.35) were calculated as in Fig. 3. (*C*) Intracellular pH detected with SNARF-1. Optical setup 3 in Table 1 was used. The ratio between the fluorescence intensities above and below 600 nm was converted to a pH value by calibrating the ratio with SNARF-1 solutions of known pH (in 100 mM of an appropriate Good's buffer; Dojindo Laboratories). The color bar for images in (*C*) represents pH (linear scale) in the range of 6.9 (violet) to 7.5 (white). (*D*) Transmission images showing the fertilization envelope recorded simultaneously with (*C*). CD pair is aligned with the AB pair using the temporal relationships established in Fig. 7 (thick solid lines with + symbols in Fig. 7 correspond to AB pair in Fig. 5).

(Fig. 5 *B*), which we interpret as the indication of membrane reorientation, and then by the rise of the fertilization envelope (Fig. 5 *D*). Detailed analysis (Fig. 6 below) showed that there was a pause followed by a second wave of membrane reorientation at ~1 min (note the asymmetry between left and right in image 1′00 in Fig. 5 *B*). Only pH (Fig. 5 *C*) changed homogeneously. (The slight inhomogeneity seen in all pH images is due to incomplete shading correction.)

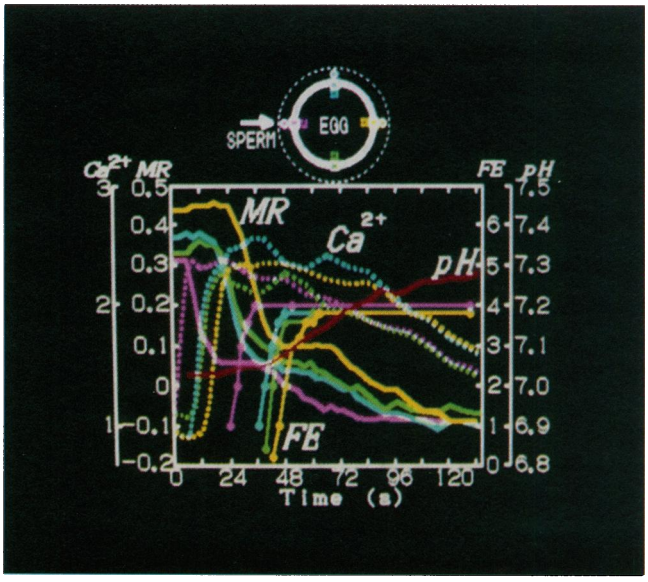

FIGURE 6 Typical spatiotemporal patterns of the four fertilization events. Changes at four points in an egg (violet, left; light blue, top; green, bottom; yellow, right), shown diagrammatically at the top, are plotted against time. Data from the same records as in Fig. 5. (Ca^{2+}) The fluorescence intensity of Calcium Green-1 (dotted line) relative to the value before insemination. (MR) Polarization of RH292 fluorescence indicating membrane reorientation (thick solid lines). Polarization values at left (shown in pink) and right (yellow) of the egg are sign inverted. (FE) Height of the fertilization envelope in μm (thin solid lines with filled circles). (pH) The fluorescence signal of SNARF-1 converted to pH values using calibration with dye solutions (single red line).

In 10 experiments where different waves were observed simultaneously in one egg, the directions of propagation always coincided with each other. Presumably, the origin of the waves was the sperm attachment site. This was directly confirmed in a few cases: a fertilizing sperm was observed in one experiment, and a fertilization cone was seen in two experiments. (In eggs of the sand dollar *S. mirabilis*, where the observation of a fertilizing sperm was easier, the coincidence between the location of the fertilizing sperm and the wave origin was confirmed five times in 13 experiments.) In Fig. 5, images in the four rows are rotated such that all waves start from the left side, although this was actually the case only for rows *A* and *B*.

Details of the time courses

From the continuous recordings shown in Fig. 5, details of the temporal sequences are reconstructed in Fig. 6. Changes at four points in the egg image, top, right, bottom, and left, are plotted with different colors as defined in the diagram at the figure top. In this plot, the waves are represented by the shift of curves toward right, from violet to green/light blue and then to yellow. The intracellular pH, which changed homogeneously, is shown in a single red line.

After the rise of $[Ca^{2+}]_i$ in the form of the calcium wave, $[Ca^{2+}]_i$ gradually decreased as seen in Fig. 6. This pattern, as well as the initial wave, was also confirmed in the ratio

images obtained with the other indicator dye indo-1 (setup 5 in Table 1, data not shown). The calcium wave was apparently much slower than the diffusional influx of external calcium into an egg whose membrane was permeabilized by electroporation (Kinosita et al, 1991), demonstrating that the chained release of calcium from internal stores during the wave requires a finite amount of time.

The polarization of RH292 fluorescence, marked MR (membrane reorientation) in Fig. 6, started to decrease before $[Ca^{2+}]_i$ reached its peak. The decrease in polarization took place in two steps, with a relatively clear pause in between. The timing of the first step coincides with that of cortical granule exocytosis and the beginning of microvillar elongation (see Discussion, below). These are temporally overlapping processes and both make the orientation of the surface membrane more random. We therefore consider that the first step reflects the exocytosis and an initial stage of microvillar elongation. In the second step, the polarization changed its sign, clearly indicating that the cell membrane now reoriented on the average into radial directions as the result of the formation of long and erect microvilli (Fig. 2 and Fig. 4 *D*). Thus, microvilli apparently grew in two steps with an intermediate pause (see Discussion). Or, the second step may reflect straightening of the initial, irregular microvilli (compare Fig. 4, *B* and *C*). As already mentioned, the second step also propagated as a wave, and its direction was the same as the first one. The two-step decrease was observed in all polarization measurements on the eggs of *A. crassispina* ($n = 12$), irrespective of whether the egg was pretreated with DTT or not. With eggs of *S. mirabilis*, the second step was observed only with eggs pretreated with DTT ($n = 7$); without DTT, the depolarization stopped after the first step ($n = 9$).

The two-step decrease in polarization was also seen in eggs of *A. crassispina* whose membrane was stained with dil (not shown). The structure of dil suggests that its chromophore will lie parallel to the membrane surface, as has been confirmed by Axelrod (1979) on erythrocyte membrane. As expected, the fluorescence of dil in unfertilized eggs was polarized perpendicular to the egg radius in contrast to RH292, whose polarization was parallel to the egg radius. Upon fertilization, the dil polarization decreased in two steps and eventually changed its sign (the final polarization was parallel to the egg radius). Both steps propagated as waves starting from the sperm attachment site. Overall, the results with dil were quite similar to those with RH292 except for the 90° difference in the direction of polarization.

The height of the fertilization envelope was judged by eye by placing a scale plate on the monitor screen. The elevation of the fertilization envelope did not always proceed uniformly over the egg surface. The initial rise from the surface nevertheless could in all cases be described as a wave starting at the sperm site.

In Fig. 6, the intracellular pH is plotted in the single red line, because the change was spatially homogeneous. Another difference, compared with the other three events, was that the rise in pH was relatively slow.

The pH images obtained with SNARF-1 were calibrated with SNARF-1 solutions of known pH. The initial pH was 6.85 ± 0.14, and the size of the pH increase was 0.29 ± 0.06 ($n = 5$). When calibration was made with egg homogenate titrated with HCl or KOH, these pH values became higher by 0.5. At present, we do not know which of the calibrations better approximates real values of intracellular pH. Shen and Steinhardt (1978) reported a rise from 6.84 to 7.26, and Whitaker and Steinhardt (1981) from 6.93 to 7.18, for *Lytechinus pictus*; Hamaguchi (1982) observed an increase of 0.4–0.5 from pH of 6.5–6.75 in eggs of the sand dollar *Clypeaster japonicus*, and Payan et al. (1983) from 7.38 to 7.64 in *Paracentrotus lividus*.

Effect of cytochalasin B on membrane reorientation

Cytochalasin B has been shown to disturb microvillar elongation (Eddy and Shapiro, 1976), presumably through interaction with actin. Its effect on the fluorescence polarization of RH292 was examined in eggs of *S. mirabilis*. As already mentioned, these eggs, when pretreated with DTT, showed a two-step decrease in polarization quite similar to that in eggs of *A. crassispina*. When the DTT-treated eggs were further treated with 20 μM cytochalasin B for 10 min, the second step of polarization decrease disappeared: after the first decrease, the polarization stopped short of reversal and remained constant for at least 2 min. The polarization values at the top, bottom, right, and left of eggs decreased from unfertilized values of 0.51 ± 0.03 to 0.15 ± 0.03 ($n = 7$, values at right and left are sign inverted), whereas without cytochalasin B the polarization changed from 0.58 ± 0.06 to -0.05 ± 0.02 by 3 min after insemination ($n = 7$). These results suggest that the second step of polarization decrease is closely associated with the reorganization of actin in microvilli.

Relationship among four waves

Fig. 7 summarizes the temporal relationships among the four waves, the rise of $[Ca^{2+}]_i$, the rise of fertilization envelope (FE), and the two steps of membrane reorientation (MR1 and MR2), observed in different eggs. Each egg gives two or three curves, plotted in the same symbol/line type, showing two of the three different signals (Ca, FE, or MR) observed simultaneously in that egg. Curves obtained from each egg (i.e., curves with the same symbol/line type) are shifted along the time axis without changing their mutual relationships, such that the curves for each of the four waves overlap maximally (as judged by eye).

The shadings in Fig. 7 emphasize that the four sets of curves are basically parallel to each other: all four waves propagated in the same direction at a common speed of about 10 μm/s. This is consistent with, although not a proof of, the scheme in which elevated $[Ca^{2+}]_i$ triggers the cortical granule exocytosis, which leads on one hand to the microvillar growth, and on the other to the formation and elevation of

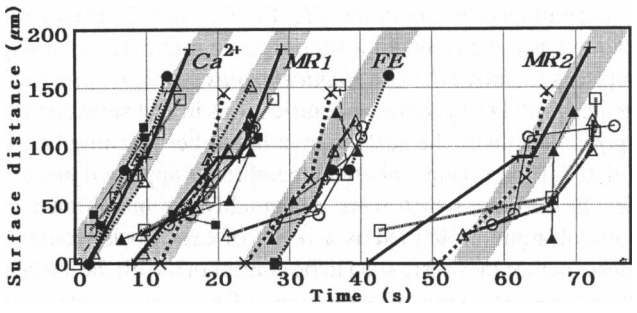

FIGURE 7 Relationship among four waves, $[Ca^{2+}]_i$, membrane reorientation (MR1 and MR2), and the elevation of fertilization envelope (FE). Each symbol in this figure represents the arrival of the wave at the top, left, bottom, or right of the egg image. The abscissa is the rising edge (falling edge for polarization) of the curve as in Fig. 6, estimated by extrapolation of the steep portion. The ordinate is the distance, along the circular edge of the egg image, between the wave origin (judged on raw images by eye) and the measurement point. Altogether 8 or 12 measurements were made on each egg, two different signals at four points. Different symbols/line types in the figure show different eggs. Some of the lines show zigzag patterns, due in part to inaccuracy in locating the wave origin and in part to non-uniform propagation of the wave. The shadings are drawn by eye such that most points for each wave fall within the shaded area.

the fertilization envelope (see, e.g., Chandler, 1991). Fig. 7 shows that the reaction(s) leading to the exocytosis/microvillar growth take ~10 s and the formation of fertilization envelope takes ~25 s after the $[Ca^{2+}]_i$ rise. A delay of ~50 s exists between the beginning of exocytosis and the second step of membrane reorientation.

The temporal characteristics of the three early waves in Fig. 7 basically agree with reported observations. The velocity of calcium wave has been studied in many species, most values falling between 5 and 15 μm/s (Jaffe, 1985). The delay between the calcium wave and the elevation of fertilization envelope has also been measured: ~30 s in *Arabacia punctulata* (Eisen et al., 1984), and 10 ± 3 s in *C. japonicus* (Hamaguchi and Hamaguchi, 1990). The wave of membrane reorientation is less well characterized, but at least the wave of exocytosis starts between calcium and fertilization envelope waves (Chandler, 1991). In *S. purpuratus*, the delay between these two events is <10 s, which is small compared with other species (Paul and Epel, 1971).

The ordinate of Fig. 7 is the distance, from the point of wave origin, along the egg surface. Thus, the surface distance, rather than the linear distance, was proportional to the elapsed time. A closer look at Fig. 7, however, reveals that the later curves are not necessarily linear with time, and tend to be upward concave. Whereas the first wave, the calcium wave, is basically a surface wave as has also been suggested by Mohri and Hamaguchi (1991), the later waves may have both surface and linear (bulk) components.

Recent studies with confocal microscopy (Stricker et al., 1992; Whitaker and Swann, 1993; Galione et al., 1993) show that the calcium wave in sea urchin eggs travels not only along the surface but also through the egg interior. The confocal images at the same time appear to indicate that the calcium wave travels faster on the surface (also see image 0′10 in Fig. 5), or that the surface wave subsequently propagates, with a delay, into the egg interior. We consider that we see this surface component of the calcium wave in Fig. 7, where we plot the times of the initial rise of $[Ca^{2+}]_i$ at each point. For the later events, the membrane reorientation and the formation of fertilization envelope, the slower, bulk wave of calcium rise may catch up and boost the surface wave. This could explain the concave curves seen in Fig. 7.

DISCUSSION

Detection of molecular orientations with unpolarized excitation

Fluorescence polarization is often used for the estimation of the rotational mobility of the fluorophore. With sand dollar eggs, for example, Hirano (1991) has shown that the mobility of probe molecules in the plasma membrane decreases upon cortical exocytosis: the exocytosis makes the membrane less "fluid." In this paper, the polarization is used for the assessment of molecular orientations, not of mobility.

In general, polarization of fluorescence indicates the orientational distribution of the fluorophores at the moment of emission: the instantaneous distribution of the emission transition moment of excited fluorophores completely determines the observed polarization. If the excitation is isotropic (oscillations in all directions) and therefore all fluorophores are excited with an equal probability, the instantaneous distribution should be an unbiased sample of the steady-state distribution. In this case, the observed polarization reflects the steady-state orientational distribution (emission moment) of the fluorophores regardless of whether they are mobile. If one is to estimate the rotational mobility, one has to create, through an anisotropic excitation (photoselection), a non-steady-state distribution of (excited) fluorophores. Then, the observed polarization will reflect this initial distribution or the final, steady-state distribution according to whether the rotational motion is slow or fast compared with the fluorescence lifetime.

Whereas the polarization under isotropic excitation is determined solely by the steady-state distribution, the polarization under anisotropic excitation involves additional factors such as the rate of rotation, fluorescence lifetime, and the angle between the emission and absorption transition moments. Isotropic excitation is preferable when steady-state distribution alone is to be examined. For example, a sample in which fluorophore orientations are completely random always gives rise to unpolarized fluorescence under isotropic excitation. Under a vertically polarized excitation, however, the same sample may exhibit vertically polarized fluorescence if the fluorophores are immobile (and the absorption and emission transition moments are parallel), or unpolarized fluorescence if the fluorophores rotate rapidly.

In the present work, we attempted to visualize membrane reorientation through the fluorescence polarization of RH292 (and diI). Our concern here was the steady-state orientational distribution of RH292, or of the membrane in which RH292 resided, and not the probe's rotational mobility in the

membrane. We therefore used unpolarized light for excitation. Although the numerical aperture of the objective used was not large enough to warrant isotropic excitation, the imbalance in excitation was along the optical axis and therefore should not have a large effect on the observed polarization in the plane perpendicular to the optical axis. Thus, the polarization reflects predominantly the steady-state orientations of the probe molecules. For example, the polarization image in Fig. 3 *D* shows that the orientation of RH292 in the unfertilized egg was highly restricted along the egg radius. Within the restriction, individual RH292 molecules may or may not have undergone rapid wobbling; the observed polarization does not discriminate between these two cases.

Membrane reorientation

The observed depolarization (toward 0) of the RH292 fluorescence upon fertilization implies that orientations of the probe molecules, initially parallel to the egg radius, became random. One interpretation could be that the orientation of RH292 became random within the cell membrane as a result of membrane fluidization. However, Hirano (1991) has indicated a decrease, rather than an increase, in fluidity upon exocytosis. Also, time-resolved fluorescence depolarization measurement (K. Kinosita Jr., unpublished data) has shown that the rotational mobility of RH292 is restricted to within a narrow angular range even in a fluid asolectin membrane. This is consistent with the general trend that the motion of a probe chromophore located closer to the surface of lipid bilayer is more restricted compared with chromophores deep inside the bilayer and is therefore less sensitive to the bilayer "fluidity" (Kinosita et al., 1984). Thus the disordering upon fertilization should, at least in large part, be in the form of membrane reorientation. That the other probe diI, whose chromophore is also situated at the bilayer surface, gave a quite similar pattern of polarization change supports this view.

The cortical granule exocytosis leads to membrane disordering: fusion of cortical granules with the cell membrane should make the orientations of the surface membrane more random, as confirmed by electron microscopy (Chandler and Heuser, 1979). This will lead to the depolarization of fluorescence, because the newly joint membranes will soon be stained with RH292 (or diI) by lateral diffusion (and, in the case of water-soluble RH292, possibly with residual RH292 in the medium). The time course of exocytosis, monitored by light scattering from an egg suspension (Paul and Epel, 1971), is similar to the first step of depolarization in Fig. 6, suggesting that exocytosis did make a significant contribution to our fluorescence signal. Also, the growth of microvilli, as diagrammed in Fig. 2, will initially be a disordering factor, because the growth tends to rotate the surface membrane into new orientations. Thus, the first step of depolarization seen in Fig. 6 may well involve these two events, which according to Chandler (1991) are temporally overlapping processes.

Preliminary observations (Y. Tanaka and H. Hakozaki, unpublished data), under a fluorescence microscope, of egg surfaces (*S. mirabilis* and *Hemicentrotus pulcherrimus*, both treated with DTT) at high magnifications in fact showed that, upon exocytosis, the surface membrane became highly undulated. Fluorescent, spherical membranes appeared just under the surface, which were presumably the membranes of cortical granules stained as a result of exocytosis; some of these membranes were seen to be continuous with the surface membrane, showing pit structures. (The fluorescence from these spherical membranes was also polarized, indicating that the dye motion was restricted also in granular membranes.) Within 20 s from the beginning of exocytosis, thin protrusions (presumably microvilli) up to a few μm in length were recognized on the surface. Longer observation has so far been unsuccessful, but these results indicate that the first step of depolarization in Fig. 6 was caused by exocytosis, which was the dominant factor in the initial stage, and microvillar growth.

The second step, the reversal of polarization, must be due to ordering into new orientations (perpendicular to the original orientations). We think that the side walls of microvilli are the only candidate for the cause of the perpendicular order. The new order arises either from a further elongation of microvilli or from straightening of irregular microvilli. The two possibilities cannot be distinguished in our polarization measurement. However, the presence of a clear pause between the two steps suggests that the second step is not a simple continuation of the first one; if it is further elongation, the driving force must be different from the first one.

The experiment with cytochalasin B suggests that the second step is driven by actin dynamics. This, together with the coincidence between the second step and the onset of pH rise (Fig. 6), conforms with the two-step scheme for microvillar growth suggested by Begg et al. (1982). These authors showed that the increase in $[Ca^{2+}]_i$ induces elongation of microvilli but the elongated microvilli remained flaccid if subsequent pH rise was inhibited. Cytoplasmic alkalinization, either during normal fertilization or by artificial means, caused bundling of actin filaments in the microvilli and converts the flaccid microvilli into erect ones. It is thus tempting to assign the second step of membrane reorientation (Fig. 6) to the pH-induced erection of microvilli. A weakness of this interpretation is that, whereas the pH rise was homogeneous, the second step propagated as a wave. This point is discussed in the next subsection.

Schroeder (1978) has shown that a second burst of microvillar elongation takes place midway between fertilization and first cell division. Presumably, this second burst occurring 60 min after insemination is unrelated to the second step we observed, because of the large time difference.

Signal pathway leading to pH rise

As already discussed, the parallelism among the four waves is consistent with the scheme that the rise in $[Ca^{2+}]_i$ triggers the later three waves. Apparently, the pH change is on a

different pathway because pH rose homogeneously. However, the homogeneous rise is not necessarily incompatible with a scheme in which alkalinization is also triggered by calcium wave.

It has been suggested that the rise in pH results from the activation of Na^+/H^+ exchanger at the egg surface (Johnson et al., 1976; Shen and Steinhardt, 1978). Then, the slow and homogeneous rise of pH without a clear pH gradient toward egg interior (Figs. 5 and 6) implies that the extrusion of H^+ across the surface membrane is slow compared with the redistribution of H^+ in the strongly buffered egg cytoplasm, which is equivalent to 60 mM phosphate (Hamaguchi, 1982). Even if the Na^+/H^+ exchanger is activated locally around the sperm attachment site in the beginning, the local efflux may well be compensated by the buffering action and subsequent diffusion in the cytoplasm, without producing a detectable pH "wave." In an egg that was activated by local application of an ionophore and that produced a partial fertilization envelope, Whitaker and Steinhardt (1981) observed homogeneous and slow rise of pH.

Diacylglycerol is implicated in the activation of the Na^+/H^+ exchanger (Swann and Whitaker, 1985), and calcium at a few μM activates phosphoinositide breakdown in egg cortex (Whitaker and Irvine, 1984). It is quite possible that calcium wave initiates the chain reactions leading to the pH rise, and that each reaction proceeds as a wave except for the final pH change, which requires massive H^+ transport.

If the above scheme applies, pH in the immediate vicinity of the cell membrane may change in a wavelike fashion despite the homogeneous rise in the bulk cytoplasm. The local change, which would be undetected in our low-resolution image, might well be significant in the thin and long microvillus and straighten it through actin bundling. The second step in the polarization change (Fig. 6) may reflect this process. Further experimentation is required to test these possibilities.

In this report, we applied multiview microscopy mainly to the examination of normal fertilization processes. The technique will be more powerful in experiments in which a defined perturbation is given to a cell to modify the normal process. To be able to see various aspects of cellular responses simultaneously and in real time should be a great advantage in disentangling complicated signal pathways.

We thank Dr. A. Ikegami (Keio University School of Medicine, Hiyoshi, Yokohama) and Dr. Y. Inoue (The Institute of Physical and Chemical Research, Wako, Saitama) for their continuous support on which this work is based. We also thank Drs. Y. Hamaguchi (Tokyo Institute of Technology, Meguro, Tokyo), S. Nemoto and M. Yamaguchi (Ochanomizu University, Tateyama, Chiba), M. Yamamoto (Okayama University, Ushimado, Okayama), and I. Yasumasu (Waseda University, Shinjuku, Tokyo) for valuable suggestions and the help in obtaining sea urchins, and Mr. M. Hosoda and Mr. K. Atsumi (Hamamatsu Photonics K. K., Hamamatsu, Shizuoka) for extensive support in developing the image-analysis system.

This work was supported by grants-in-aid from the Ministry of Education, Science and Culture of Japan, and by Special Coordination Funds for Promoting Science and Technology from the Agency of Science and Technology of Japan.

REFERENCES

Axelrod, D. 1979. Carbocyanine dye orientation in red cell membrane studied by microscopic fluorescence polarization. *Biophys. J.* 26:557–574.

Begg, D. A., L. I. Rebhun, and H. Hyatt. 1982. Structural organization of actin in the sea urchin egg cortex: microvillar elongation in the absence of actin filament bundle formation. *J. Cell Biol.* 93:24–32.

Berridge, M. J. 1993. Inositol triphosphate and calcium signalling. *Nature (Lond.).* 361:315–325.

Chambers, E. L., and J. de Armendi. 1979. Membrane potential, action potential and activation potential of eggs of the sea urchin, *Lytechinus variegatus. Exp. Cell Res.* 122:203–218.

Chandler, D. E. 1991. Multiple intracellular signals coordinate structural dynamics in the sea urchin egg cortex at fertilization. *J. Electron Microsc.* 17:266–293.

Chandler, D. E., and J. Heuser. 1979. Membrane fusion during secretion. Cortical granule exocytosis in sea urchin eggs as studied by quick-freezing and freeze-fracture. *J. Cell Biol.* 83:91–108.

Eddy, E. M., and B. M. Shapiro. 1976. Changes in the topography of the sea urchin egg after fertilization. *J. Cell Biol.* 71:35–48.

Eisen, A., D. P. Kiehart, S. J. Wieland, and G. T. Reynolds. 1984. Temporal sequence and spatial distribution of early events of fertilization in single sea urchin eggs. *J. Cell Biol.* 99:1647–1654.

Epel, D., A. M. Weaver, and D. Mazia. 1970. Methods for removal of the vitelline membrane of sea urchin eggs. *Exp. Cell Res.* 61:64–68.

Galione, A., A. McDougal, W. B. Busa, N. Willmott, I. Gillot, and M. Whitaker. 1993. Redundant mechanisms of calcium-induced calcium release underlying calcium waves during fertilization of sea urchin eggs. *Science (Washington DC).* 261:348–352.

Hamaguchi, M. S. 1982. The role of intracellular pH in fertilization of sand dollar eggs analyzed by microinjection method. *Dev. Growth & Differ.* 24:443–451.

Hamaguchi, Y., and M. S. Hamaguchi. 1990. Simultaneous investigation of intracellular Ca^{2+} increase and morphological events upon fertilization in the sand dollar egg. *Cell Struct. Funct.* 15:159–162.

Hirano, K. 1991. Changes in membrane fluidity of sand dollar egg cortices caused by Ca^{2+}-induced exocytosis: microscopic analysis with fluorescence anisotropy. *Dev. Growth & Differ.* 33:451–458.

Jaffe, L. F. 1985. The role of calcium explosions, waves, and pulses in activating eggs. *In* Biology of Fertilization, Vol. 3. C. B. Metz, and A. Monroy, editors. Academic Press, Tokyo. 127–165.

Johnson, J. D., D. Epel, and M. Paul. 1976. Intracellular pH and activation of sea urchin eggs after fertilisation. *Nature (Lond.).* 262:661–664.

Kay, E. S., and B. M. Shapiro. 1985. The formation of the fertilization membrane of the sea urchin egg. *In* Biology of Fertilization, Vol. 3. C. B. Metz, and A. Monroy, editors. Academic Press, Tokyo. 45–80.

Kinosita, K. Jr., H. Itoh, S. Ishiwata, K. Hirano, T. Nishizaka, and T. Hayakawa. 1991. Dual-view microscopy with a single camera: real-time imaging of molecular orientations and calcium. *J. Cell Biol.* 115:67–73.

Kinosita, K. Jr., S. Kawato, and A. Ikegami. 1984. Dynamic structure of biological and model membranes: analysis by optical anisotropy decay measurement. *Adv. Biophys.* 17:147–203.

Mohri, T., and Y. Hamaguchi. 1991. Propagation of transient Ca^{2+} increase in sea urchin eggs upon fertilization and its regulation by microinjecting EGTA solution. *Cell Struct. Funct.* 16:157–165.

McCulloh, D. H., and E. L. Chambers. 1992. Fusion of membranes during fertilization: increase of sea urchin egg's membrane capacitance and membrane conductance at the site of contact with the sperm. *J. Gen. Physiol.* 99:137–175.

Paul, M., and D. Epel. 1971. Fertilization-associated light-scattering changes in eggs of the sea urchin *Strongylocentrotus purpuratus. Exp. Cell Res.* 65:281–288.

Payan, P., J.-P. Girard, and B. Ciapa. 1983. Mechanism regulating intracellular pH in sea urchin eggs. *Dev. Biol.* 100:29–38.

Schroeder, T. E. 1978. Microvilli on sea urchin eggs: a second burst of elongation. *Dev. Biol.* 64:342–346.

Schroeder, T. E. 1979. Surface area changes at fertilization: resorption of the mosaic membrane. *Dev. Biol.* 70:306–326.

Schuel, H. 1985. Functions of egg cortical granules. *In* Biology of Fertilization. Vol. 3. C. B. Metz, and A. Monroy, editors. Academic Press, Tokyo. 1–43.

Shen, S. S., and R. A. Steinhardt. 1978. Direct measurement of intracellular pH during metabolic derepression of the sea urchin egg. *Nature (Lond.).* 272: 253–254.

Steinhardt, R. A., L. Lundin, and D. Mazia. 1971. Bioelectric responses of the echinoderm egg to fertilization. *Proc. Natl. Acad. USA.* 68:2426–2430.

Stricker, S. A., V. E. Centonze, S. W. Paddock, and G. Schatten. 1992. Confocal microscopy of fertilization-induced calcium dynamics in sea urchin eggs. *Develop. Biol.* 149:370–380.

Swann, K., and M. Whitaker. 1985. Stimulation of the Na/H exchanger of sea urchin eggs by phorbol ester. *Nature (Lond.).* 314: 274–277

Whitaker, M., and R. F. Irvine. 1984. Micro-injection of inositol trisphosphate activates sea urchin eggs. *Nature (Lond.).* 312:636–639.

Whitaker, M. J., and R. A. Steinhardt. 1981. The relation between the increase in reduced nicotinamide nucleotides and the initiation of DNA synthesis in sea urchin eggs. *Cell.* 25:95–103.

Whitaker, M., and K. Swann. 1993. Lighting the fuse at fertilization. *Development.* 117:1–12.